*Physics – Uspekhi* **40** (11) 1175 – 1187 (1997) 

*INSTRUMENTS AND METHODS INVESTIGATION* PACS numbers: 61.14.Hg, 61.16. Di, 68.55.Bd

# Atomic structures on a GaAs(001) surface grown by molecular beam epitaxy

R Z Bakhtizin, T Hashizume, Q-K Xue, T Sakurai

## Contents

**1. Introduction** **1175**
**2. Atomic structures on a GaAs(001) surface** **1176**
**3. Experimental** **1177**
3.1 Molecular-beam epitaxy chamber in line with the scanning tunneling microscope; 3.2 Preparation of $2 \times 4$ and $c(4 \times 4)$ phases; the migration-enhanced epitaxy technique; 3.3 Surface structure studies using reflection high-energy electron diffraction; 3.4 STM studies
**4. Results and discussion** **1179**
4.1 STM images of the $2 \times 4-\alpha$, $\beta$, and $\gamma$ phases; 4.2 Dynamical RHEED analysis of the $2 \times 4-\alpha$, $\beta$, and $\gamma$ phases; 4.3 Surface phase transitions between the $c(4 \times 4)$ and $2 \times 4-\gamma$ lattices
**5. Structural models for the two-dimensional $2 \times 4-\alpha$, $\beta$ and $\gamma$ phases** **1185**
**6. Conclusions** **1185**
**References** **1186**

**Abstract. A unique apparatus for *in-situ* atomic-resolution study of solid state structures grown by molecular beam epitaxy (MBE) is developed, in which a scanning tunneling microscope (STM) is combined with an MBE chamber within the same vacuum system. The utility of the apparatus is demonstrated by examining atomic structures on a molecular-beam-epitaxial GaAs(001) surface over a wide range of [As]/[Ga] ratios. By varying the As surface coverage, the $2 \times 4-\alpha$, $\beta$, $\gamma$ and $c(4 \times 4)$ phases are examined in detail. High-resolution STM images indicate that $2 \times 4-\alpha$, $\beta$ and $\gamma$ phases in the outermost surface layer have essentially the same unit cell consisting of two As dimers and two As dimer vacancies. Using the STM images, reflection high-energy electron diffraction (RHEED) patterns and dynamical RHEED calculations, the existing structural models for the $2 \times 4$ phases are analysed and a new model of the As-rich GaAs(001) surface is proposed, found to be consistent with most of the previous observations.**

**R Z Bakhtizin** Department of Physical Electronics, Bashkir State University, 450074 Ufa, Russia
Tel./Fax (7-3472) 503 085
E-mail: raouf@online.ru
**T Sakurai, Q-K Xue** Institute for Materials Research (IMR), Tohoku University, Sendai 980-77, Japan
Tel. +81-22-215-2021
Fax +81-22-215-2020
E-mail: sakurai@apfim.imr.tohoku.ac.jp
**T Hashizume** Hitachi Advanced Research Laboratory, Hitachi, Ltd., Hatoyama, Saitama 350-03, Japan
Tel. +81-492-96-8111
Fax +81-492-96-6006
E-mail: tomi@harl.hitachi.co.jp

Received 17 March 1997, revised 10 June 1997
*Uspekhi Fizicheskikh Nauk* **167** (11) 1227 – 1241 (1997)
Translated by E G Strel'chenko; edited by M S Aksent'eva

## 1. Introduction

Molecular-beam epitaxy (MBE) is currently the most promising technique for the growth of solid state structures and in particular in the fabrication of opto-electronic and microwave devices involving submicron size single crystal structures of layers of different elemental composition and similar lattice constants [1, 2]. Basically, MBE is the deposition of modulated molecular (atomic) beams on a single crystal substrate held at an elevated temperature in an ultrahigh vacuum. In such epilayers both the composition and doping level depend on the relative supply rates of the components and dopants. Growth normally proceeds at 1 to 3 $\mu$/h ($\sim$ 1 monolayer/s), slow enough to allow the impinging particles to diffuse quite rapidly over the growing surface, which enables thin film growth to be controlled to a high (up to atomic) accuracy. Needless to say, the fabrication of high-quality epilayer structures (or reconstructions) crucially depends on the close monitoring of the surface structure and stoichiometry and requires the study of the microscopic crystal growth processes involved.

Because MBE requires ultrahigh vacuum conditions, epitaxial growth is usually monitored *in situ* using traditional diagnostic techniques such as reflection high energy electron diffraction (RHEED), low energy electron diffraction, or Auger-electron spectroscopy [3]. In many cases, however — particularly during the initial, most important, growth stages — these techniques do not have sufficient resolution to identify the structures produced and growth types involved, and must therefore be replaced by scanning tunneling microscopy (STM), which is the most efficient among the real-space, atomic-resolution techniques currently in use for the diagnostics of solid state nanosize structures [4]. Earlier attempts of this kind, however, involved transferring the sample from the MBE chamber through air to the STM system. We were able, after overcoming many difficulties in

our way, to develop a more suitable scheme in which the ultrahigh vacuum STM is combined with the MBE chamber within the same vacuum system.

It is the purpose of the present review to describe this combined MBE-STM system and to illustrate its application to the *in situ* study of atomic structures on an MBE-grown As-rich GaAs(001) surface.

## 2. Atomic structures on an GaAs(001) surface

Atomic structures that form on an MBE-grown GaAs(001) surface have been the subject of intense research in the last two decades both because of their continuing scientific interest [5–20] and for technological reasons (it is on this crystal face where many nanoobjects, such as quantum dots, quantum wires, etc., as well as most GaAs-based devices are grown by MBE). As the surface energy is lowered, GaAs(001) exhibits many low-dimensional nanostructures, which may be quite complicated and between which structural phase transitions occur; all these effects depend on the surface stoichiometry and can be controlled by varying the treatment conditions (the sample temperature and the [Ga]/[As] MBE flux ratio) [3–5]. The reconstructions observed on GaAs(001) range from the most As-rich phase $c(4\times4)$, $2\times4/c(2\times8)$, $2\times6,\ldots$ to the Ga-rich phase $4\times2/c(8\times2)$, $4\times6$, etc., depending on the surface coverage and MBE conditions. The MBE reconstructions are extremely sensitive to the stoichiometry of the top layer because the structure of the polar face GaAs(001) is strongly dependent on the cation–anion ratio. The top layer stoichiometry and structure have been investigated by a variety of surface-sensitive techniques, including reflection high energy electron diffraction (RHEED) [9–20], low energy electron diffraction and Auger-electron spectroscopy [21, 25], photoelectron spectroscopy [26–28], work function measurement [25], X-ray diffraction [29], X-ray photoelectron diffraction [30], reflectance-difference spectroscopy [31], the electron energy loss spectroscopy [32], secondary electron intensity measurement [33], medium-energy ion scattering [34], and scanning tunneling microscopy [35–43]. Since MBE crucially depends on the As content, the As-rich $2\times4$ and $c(4\times4)$ phases were studied most extensively. Somewhat later, GaAs(001) band structure calculations [44–48] were employed to assess various surface structures from the surface energy minimization point of view.

Based on the experimental and theoretical work mentioned above, some general ideas about the structure of GaAs(001)–$2\times4$–As surface have emerged. Note that in the case of an 'ideal' unreconstructed GaAs(001)–$2\times4$ surface (when the surface structure is identical to the bulk structure), each surface As atom must have two dangling bonds, which is energetically unfavorable. Therefore two neighboring As atoms form a dimer along the $\langle\bar{1}10\rangle$ direction, with the consequence that the surface reconstructs with a $(2\times)$ periodicity in a manner analogous to the Si(100) surface. As a result, each As-dimer pair has two dangling bonds whose energy levels may be found from the atomic *s* and *p* levels based on the Harrison diagram [49]. According to this latter, the As dangling-bond level lies below the valence band maximum and is filled, whereas the Ga dangling-bond level is above the conduction band minimum and is empty. Although it was possible to attempt to derive the fourfold periodicity along $\langle110\rangle$ from the asymmetry of As dimers [26, 27], Chadi [44] advanced the 'missing As dimer' idea which was supported by later STM experiments [35]. The formation of dimer vacancies was considered by Chadi as a way to avoid the energetically unfavorable charge accumulation phenomenon [12]. The simplest $2\times4$ unit cell capable of maintaining electrical neutrality can be obtained by removing one out of four As dimers [50].

Although it is generally accepted that the $2\times4$ structure consists of As dimers and missing As-dimers, alternative $2\times4$ models, allowing for Ga presence in the top layer, exist. Chadi, who was the first to propose an As dimer vacancy model on the basis of tight-coupling total-energy calculations, suggested two ways for the vacancies to arrange themselves in the top near-surface layer: (a) three As dimers and one missing dimer in a unit cell (Fig. 1a), and (b) two As dimers and two dimer vacancies in one structural element (Fig. 1b) in the outer layer [44] (in this latter case, one of the Ga pairs must also be absent in the second layer). Although calculations showed that both models have nearly the same energy stability, model (b) was later rejected by Larsen [14] for growth kinetics reasons. Chadi's later version of the dimer vacancy model, with all four Ga pairs retained in the second layer (Fig. 1c), was also abandoned on the grounds that its total energy per unit cell is 1.6 eV larger than in (a) and (b).

Frankel and coworkers [32] investigated electronic energy loss spectra for atomic oxygen chemosorbed on $c(2\times8)$ GaAs(001) and found that in this case both Ga–H and As–H are present on the surface thus clearly indicating the existence of As-dimer vacancies. Based on this study, two models were proposed, one Chadi-type As vacancy model with a different surface stoichiometry; and the other involving dimerisation of the second Ga layer but having no surface relaxation [32].

Unequivocal evidence for the As vacancy model of the $2\times4$ phase was already found in the first STM experiments by Pashley et al. [35]. In those, samples prepared in a separate MBE chamber were capped by a protecting amorphous As layer before being exposed to the air, and this layer was later removed by briefly heating the sample in the STM chamber. STM images showed that the $2\times4$ periodicity is due to the regular arrays of As dimers and As dimer vacancies and that $c(2\times8)$ forms from $2\times4$ owing to the presence of an antiphase boundary along $\langle\bar{1}10\rangle$. Analysis of the STM images of the $2\times4$ cell showed them to be best explained by Chadi's three As-dimer model (Fig. 1a). Later, Biegelsen et al. [36] prepared samples *in situ* in the MBE chamber and found the top layer $2\times4$ cell to consist of three As dimers, in agreement with Pashley's [35] observation. However, when annealed longer or at higher temperatures, or at a lower $[As_4]$/[Ga] ratio, it was observed by Biegelsen and coworkers [36] that the $2\times4$ structure may have two As dimers in the top layer [36].

Larsen and Chadi [14] in discussing model selection criteria suggested that, along with Bragg's reflections, the amplitude structure of fractional-order RHEED diffraction features be taken into account. Their kinematic calculations showed that if only As atoms on the external side of the top layer are considered, then the models of Fig. 1b and 1c yield weak (0 2/4) reflections. Somewhat later, a systematic study of all previous RHEED results carried out by Farrel and Palmström (FP) [15] suggested that within the $2\times4$ reconstruction three phases ($\alpha$, $\beta$ and $\gamma$) be distinguished, depending on the 1/4, 2/4, and 3/4 RHEED intensities and on the preparation conditions [15]. From the FP analysis, for the $\alpha$ phase the 2/4 order reflection was weak relative to 1/4 and

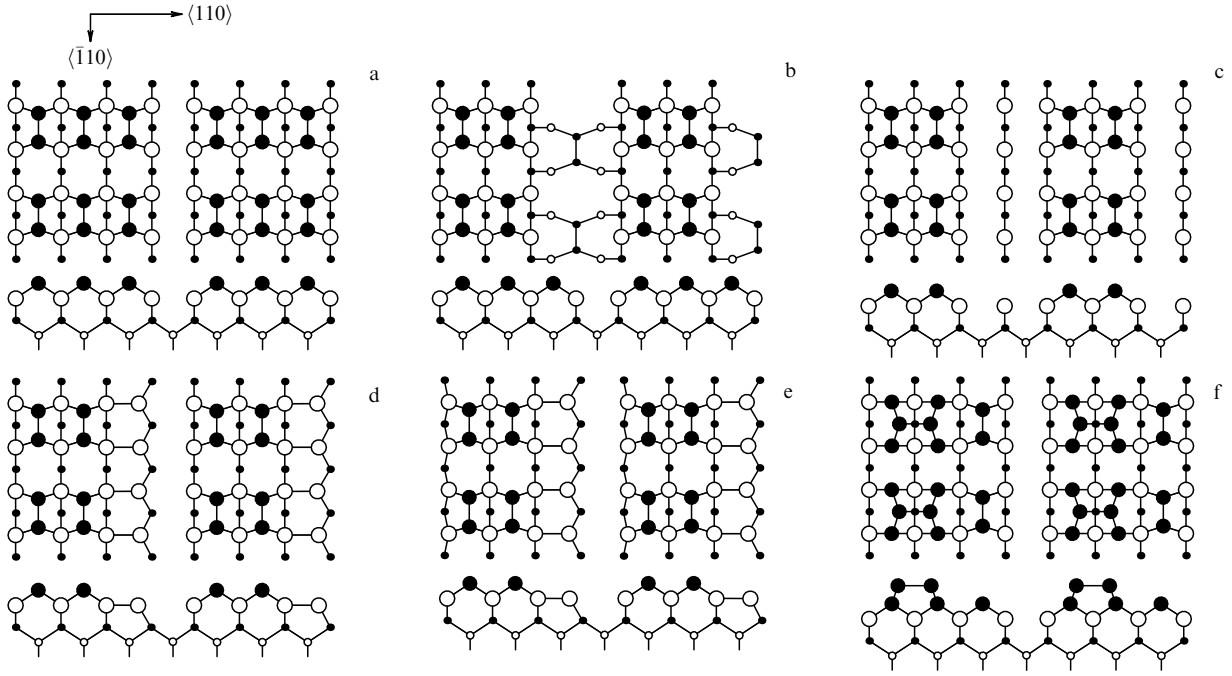


**Figure 1.** Basic structural models for the GaAs(001) – 2 × 4 surface. (a) Three As dimers, Chadi's [44]; (b) two As dimers, Chadi's [44]; (c) unstable two As dimers, Chadi's [44]; (d) two As dimers for the 2 × 4 – α phase, Farrell and Palmström [15]; (e) the same as (d) modified to include the relaxation of the second Ga layer, Northrup and Froyen's [42]; (f) an extra As dimer for 2 × 4 – γ, Farrell and Palmström [15]. Filled (open) circles denote As (Ga) atoms. Top and side views are shown for each model. As coverages are (in monolayers): 0.75 (a), 0.75 (b), 0.5 (c), 0.5 (d), 0.75 (e), and 1.0 (f).

3/4; for the β phase, it was stronger and equal in intensity to 1/4 and 3/4; for γ, it was found to vanish. In order to confirm these data, Farrell and Palmström carried out a computation of kinematic RHEED intensities and proposed a unit cell model for the α, β, and γ phases in the outer layer (the so-called FP scheme) in which the α phase consists of two As dimers (Fig. 1d, with the second Ga layer dimerised). Later Northrup and Froyen (NF) [47] introduced the relaxation displacement of the second-layer Ga atoms to enhance the stability of this model (Fig. 1e). The β unit cell in the FP scheme is in fact described by the three-dimensional model of Chadi (Fig 1a), and the γ phase, by a model with an extra ⟨110⟩-oriented As dimer on the surface of the β phase as shown in Fig. 1f [15]. In the FP scheme, the As coverage for the α, β, and γ phases should be 0.5, 0.75, and 1.0 monolayer, respectively, consistent with the values originally assumed based on preparation conditions for each phase.

The FP scheme has been in wide use since its publication, the exact number of dimers (three or two) in the model depending on the experimental conditions used and the results obtained. Thus, the important problem of the GaAs(001) – 2 × 4 structure appeared to be solved [17 – 20, 31, 46, 47]. Most recently, however, *in situ* STM experiments by Heller and Lagally [38] led them to conclude that the top layer is dominated by a two As-dimer unit cell and that a cell with three such dimers can only exist under special conditions. This was supported by experiments by Wassermeier and Bressler-Hill [39] who also showed the two As-dimer cell to be dominant. However, Gallagher and colleagues [40] saw evidence of a three As-dimer cell in their STM images. Finally, a series of medium-energy ion spectroscopy experiments on GaAs(001) grown by MBE outside the analytical chamber led Falta et al. [34] to an unorthodox model in which both Ga and As atoms are allowed in the first layer of the 2 × 4 phase.

Recognizing that the problem thus remains unsolved — and fully aware of its extreme importance — we carried out a systematic structural study of the 2 × 4 – α, β, and γ phases on the GaAs(001) surface taking advantage, in doing so, of the combined MBE-STM unit we developed earlier [41 – 43]; and compared the results with those of other workers and with existing structural models. In many cases we also employed the migration-enhanced epitaxy (MEE) technique [51] which allows the surface stoichiometry to be controlled over the entire range from As-rich to Ga-rich material.

By analyzing the high-resolution STM images and RHEED patterns of the GaAs(001) surface and comparing them with dynamical RHEED computations including multiple scattering effects, we were able to develop a unified 2 × 4 model consisting of two As dimers and two dimer vacancies in the top layer [43].

## 3. Experimental

### 3.1 Molecular-beam epitaxy chamber in line with the scanning tunneling microscope

Experiments were performed using a combination we designed for the purpose, of an ultrahigh-vacuum field ion – scanning tunneling microscope [52] and a special-design ULVAC MBE chamber with RHEED facilities for the express-control and monitoring of growth on the substrate [53]. The view of the unit is shown in Fig. 2. The MBE chamber contains six Knudsen cells, each with its own shutter and under independent microcomputer control. Two vertical 90°-rotated, mechanical, transport units (marked by an

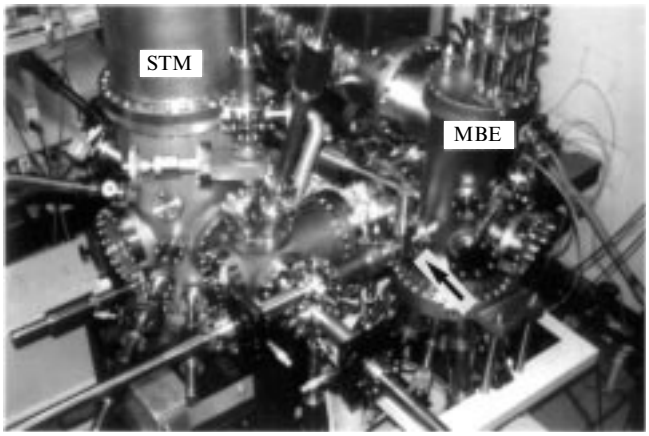


**Figure 2.** General view of the combined unit consisting of the ultra-high-vacuum scanning tunneling microscope and the molecular beam epitaxy chamber. The arrow shows the unit for transferring the sample between the STM and MBE systems.

arrow) secured rapid vacuum-conserving transfer of the sample between the MBE and STM systems. A base pressure of $4 \times 10^{-11}$ and $1 \times 10^{-10}$ Torr was maintained in the STM and MBE chambers, respectively. The scanning tip quality, crucial for atomic resolution observation, was monitored on an atomic scale using a built-in miniature field ion microscope [52, 54], which was especially important in view of the fact that the As vapor was at high pressure and could therefore reach the probe surface.

Si-doped ($1 \times 10^{18}$ cm$^{-3}$) n-type GaAS(001) samples $4 \times 10$ mm$^2$ in size were cut from wafers of appropriate crystal orientation. After chemical etching in a standard 4:1:1 mixture of $H_2SO_4 : H_2O_2 :$ DI $H_2O$, the samples were fixed to a Ta holder using In solder and then allowed to outgas in the MBE chamber for $\simeq 10$ hours at 400 °C. After the oxide surface layer was removed by annealing in the $As_4$ flux at 600 °C [7, 9], the conventional MBE technique was employed at the (optimal) growth temperature of 540 to 630 °C, growth rate of 0.15 μm/h, and $[As_4]/[Ga] \approx 30$ to produce a buffer n-type GaAs layer 0.5–1.0 μm thick (also doped with Si). To monitor the growth process, RHEED intensity oscillations [2, 3, 7] were measured. The high cooling rate of the apparatus enabled a variety of surface phases to be examined *in situ* with STM during the process of their growth. The rapid cooling of a sample was achieved by rapidly removing it (together with the holder) from the MBE chamber and transferring to the STM chamber, a procedure which did not usually take more than 2 or 3 s. The holder was cooled at $\approx 50$ °C/s as measured by an infrared pyrometer. The Si doping level was calibrated using a secondary ion mass-spectrometer and maintained at $\leqslant 1.5 \times 10^{18}$ cm$^{-3}$ in order to minimize the concentration of dopant-produced surface defects [37].

### 3.2 Preparation of $2 \times 4$ and c($4 \times 4$) phases; the migration-enhanced epitaxy technique

Using a sample preparation technique similar to Farrell and Palmström's, fractional order (1/4, 2/4, and 3/4) RHEED features generally consistent with the results of Ref. [15] were obtained. The most stable phase of all, β, was prepared by annealing the substrate at a growth temperature of 530–630 °C and holding the flux $As_4$ density constant until the intensity of the 2/4 feature increased to about that of 1/4 and 3/4. To prepare the c($4 \times 4$) and $2 \times 4$ phases, the following three procedure were used (see Table):

(1) Phases α, β and c($4 \times 4$) were obtained by annealing the substrate, originally with signs of the β phase, for several minutes at a fixed $As_4$ flux at 640, 510, and below 490 °C, respectively. Given the high pressure of As vapor, the c($4 \times 4$) phase is expected to be most rich in As.

(2) The α, β and γ phases could also be obtained from c($4 \times 4$) by heating the substrate at the respective temperatures of 300, 390, and 460 °C — but in the absence of an $As_4$ flux [36].

(3) The above phases were also produced by using the migration-enhanced epitaxy (MEE) technique of Horikoshi et al. [51] in parallel with conventional MBE. In the MEE regime (Fig. 3), $As_4$ and Ga atoms are supplied to the substrate in turn by alternately opening the As and Ga shutters, which reduced the Ga diffusion length by as much

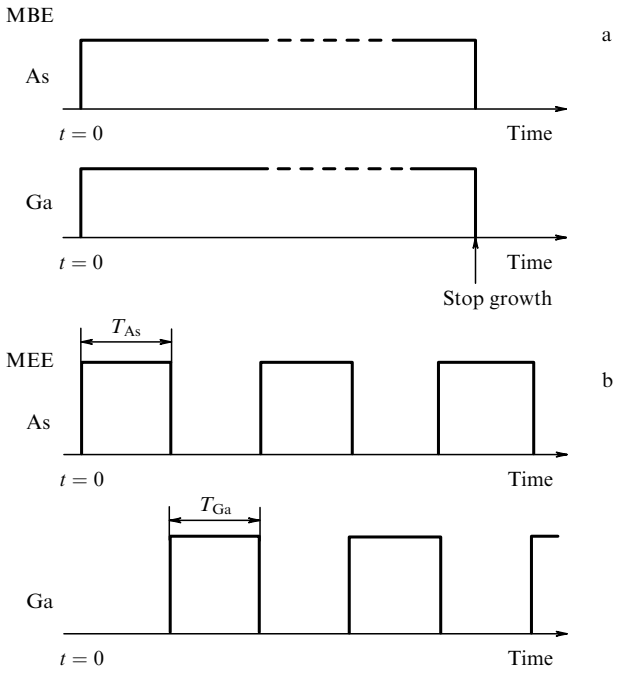


**Figure 3.** Shutter operation time regime for As and Ga Knudsen cells for (a) molecular beam epitaxy and (b) migration-enhanced epitaxy.

**Table**. Sample preparation techniques†

| Technique | α phase | β phase | γ phase | c($4 \times 4$) phase |
|---|---|---|---|---|
| Annealing in a $As_4$ flux | 640 °C | 530–630 °C | 510 °C | 490 °C |
| Annealing c($4 \times 4$) without an $As_4$ flux | 460 °C | 390 °C | 300 °C | — |
| MEE at 500 °C | — | — | $As_4/Ga = 12:1$ | $As_4/Ga = 20:1$ |

† Buffer layer: $[As_4]/[Ga]$ flux concentration $\approx 30$; growth rate 0.15 μm/h; growth and oxide-desorption temperature 600 °C.

as $\sim 10$ times compared to normal MBE: $L_{Ga} = L_{\text{without As}}/L_{\text{with As}} = 9.5$. This makes MEE very promising because the resulting surface profile is smooth enough to observe the atomic structure with STM immediately following the abrupt cooling of the sample after growth [42].

Because of the high As vapor pressure, the sample temperature and the $[As_4]/[Ga]$ flux ratio both have a very strong influence on the stoichiometry of the surface layer. For example, in method (3) Ga and As atoms are supplied to the surface simultaneously during growth, whereas in (2) As atoms are continuously desorbed from the surface, and in (1) the surface is exposed to a stationary flux of $As_4$. On the other hand, all three of these methods require a significant As and Ga transfer to the surface as well as atomic migration along the surface. Once the As atoms reaching the surface start migrating along it, the second layer Ga atoms come to the sample-vacuum interface and become highly mobile there. One would therefore expect that preparing the $c(4 \times 4)$ and $2 \times 4$ phases involves quite rapid surface migration of As and Ga atoms. Thus, high-quality large-domain surfaces could be grown at relatively low temperatures, with the surface stoichiometry being simultaneously controlled by varying the shutter operation times, $T_{As}$ and $T_{Ga}$ (see Fig. 3). The sequence of STM images in Fig. 4 shows how the GaAs(001) surface changes as the $[As_4]/[Ga]$ ratio changes from 20:1 for $c(4 \times 4)$ (Fig. 4a) to 15:1 for a mixture of $2 \times 4$ and $\gamma$ (Fig. 4d) at a sample temperature of 500 °C [42]. In a similar way, the $2 \times 4-\gamma$ phase was obtained at a $[As_4]/[Ga]$ ratio of 12:1.

### 3.3 Surface structure studies using reflection high-energy electron diffraction

To carry out a quantitative theory/experiment comparison, an outside photometric system consisting of a calibrated selective-point-input photoelectron multiplier and a fiber optic path was employed, which allowed the RHEED intensities to be measured. Along with the total intensity, its angular distribution or, in other words, intensity profiles were obtained. As these were found to be essentially the same during the (high-temperature) preparation process and after the STM study (at room temperature), the implication is that the quenching rate was sufficiently high given the low heat capacity of the sample holder. The kinetic energy of the electron beam was $\sim 10$ keV and the angle of incidence (azimuth) was taken to be $1.6° \pm 0.2°$ relative to $\langle \bar{1}10 \rangle$. The use by FP [15] of an incidence angle of 0.07° (i.e., 1.3 mrad) to reduce undesirable multiple scattering effects is somewhat doubtful because the simple relation between the incidence angle and the RHEED intensity suggests that an incidence angle of at least 1.2° is needed to obtain 3/4 or higher-order reflections. At smaller angles the Ewald sphere overlaps the reciprocal lattice vectors of the zeroth Laue zone even less, and at about 1°, when the zeroth zone virtually touches the Ewald sphere, thin elongated reflections appear which in fact are image segments of the reciprocal lattice vectors. In this case the reflections from the zeroth Laue zone can only be seen if the broadening of the reciprocal lattice vectors due to the surface imperfections is sufficient for them to intersect the Ewald sphere. But then relative reflection intensities cannot be analyzed reliably because the Ewald sphere does not cross the centers of the reciprocal lattice vectors. It is for this reason that an incidence angle of 1.6° was chosen in this work [49].

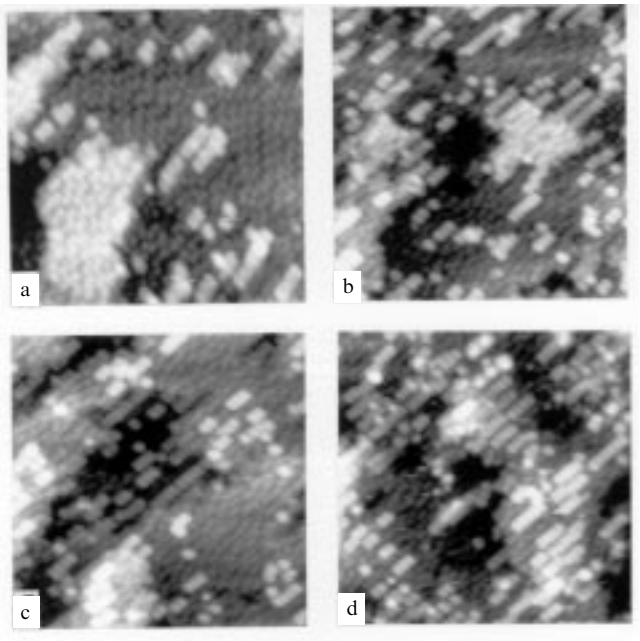


**Figure 4.** Sequence of STM images obtained for the transition of the As-rich $c(4 \times 4)$ phase to the $\gamma$ phase using an MEE technique capable of controlling the GaAs surface stoichiometry. The $[As_4]/[Ga]$ flux ratios are (a) 20:1; (b) 18:1; (c) 17:1; (d) 15:1. Tip bias $V_s = -2.5$ V, tunneling current $I_t = 2.0 \times 10^{-11}$ A, area 260 A × 260 A.

### 3.4 STM studies

Details of the STM technique are given elsewhere [52, 54]. All STM images were taken with the sample held at $V_s = -3.5$ to $-2.0$ V relative to the grounded tip and at a constant tunneling current $I_t = 2 \times 10^{-11}$ A = 20 pA. The area scanned usually ranged between 20 and 12000 $A^2$. It was repeatedly found that tunneling to unfilled sample states ($V_s > 0$) is either unstable or, in contrast with GaAs(110) [55], only acts to lower resolution for the As-rich $2 \times 4$ phase on GaAs(001) — the more so the lower the doping level. These features were first noted and discussed by Pashley [35]. In the work of Wassermeier [39], the $2 \times 4$ phase on the surface of a Be doped p-type GaAs sample was imaged in the so-called dual mode regime, with the bias voltage changing alternately from positive to negative. Wassermeier showed this to be due to the location difference between the pinning-held Fermi level and the tip related band bending. In this case, it is believed [39, 40] that the filled states contribute to the tunneling current via lone pair states localized on As dimers.

## 4. Results and discussion

### 4.1 STM images of the $2 \times 4-\alpha$, $\beta$, and $\gamma$ phases

Figure 5a–c are typical STM images of the $2 \times 4-\alpha$, $\beta$, and $\gamma$ phases, the insets showing the magnified areas of the GaAs(001)–$2 \times 4$ surface and characteristic scanning profiles taken along $\langle 110 \rangle$. The bright steps in the images lie along the $\langle \bar{1}10 \rangle$ direction a distance $d = 4\mathbf{a}_0$ apart ($\mathbf{a}_0 = 4.0$ A being the unit distance along $\langle 110 \rangle$ on the GaAs(001)–$1 \times 1$ surface) and are $2\mathbf{a}_0$ apart in the $\langle \bar{1}10 \rangle$ direction, thus forming a $2 \times 4$ structure with a unit cell $8 \times 16$ $A^2$ in size [35–40]. We believe that the dark lines between the bright steps are As-dimer vacancy regions, which is not inconsistent with Pashley's view [35].

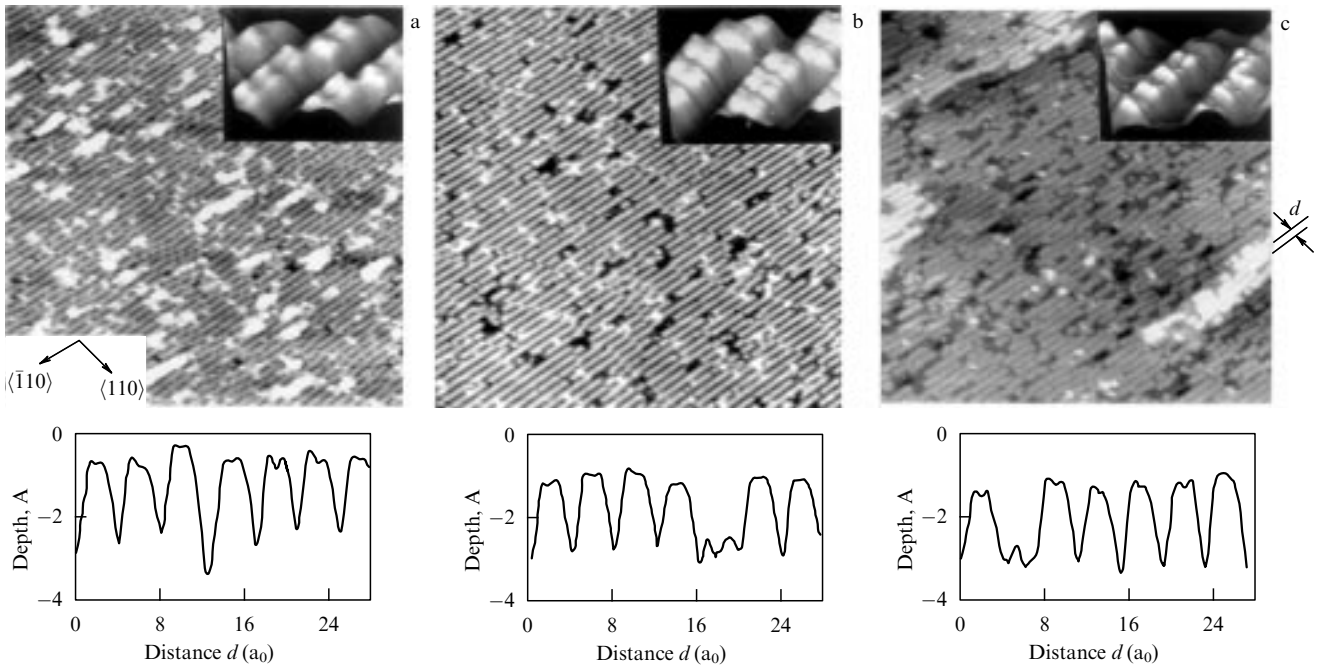


**Figure 5.** Typical STM images of the α (a), β (b), and γ (c) phases on the GaAs(001) – 2 × 4 surface (area 600 A × 900 A). Scanning profiles along the ⟨110⟩ direction and the three-dimensional magnification of some image details are shown in the insets. 2 × 4 unit cells in all three phases consist of two As dimers and two missing dimers; $V_s = -3.0$ V, $I_t = 2.0 \times 10^{-11}$ A.

Of the defect types discussed earlier [35], we observed the following three:

(1) full As-dimer vacancies forming dark regions $2\mathbf{a}_0$ apart along the $\langle\bar{1}10\rangle$ direction;

(2) the shift of 2 × 4 cells by $\mathbf{a}_0$ along $\langle\bar{1}10\rangle$, responsible for c(2 × 8) formation;

(3) the shift of 2 × 4 cells by $\mathbf{a}_0$ along ⟨110⟩, which produces a sequence of step kinks and forms a domain boundary with 4× periodicity outside the phase. Type (1) defects give rise to 2 × 4 cells a distance $d = 8\mathbf{a}_0$ apart along ⟨110⟩ (the quantity $d$ is defined in Fig. 5c). The formation of 2 × 4 cells separated by $d = 3\mathbf{a}_0$ and $5\mathbf{a}_0$ may only involve those kinks [i. e., those type (3) defects] which are not aligned along ⟨110⟩.

Both the magnified STM images and the corresponding scanning profile contours (see insets to Fig. 5) show clearly that the unit cells of the α, β and γ phases and of the 2 × 4 structure in the top layer consist of two As dimers and two dimer vacancies [43]. Our detailed analysis shows, however, that the step spacing is about 15% in excess of the expected $\mathbf{a}_0$. Since STM images reflect the distribution of the electronic density of states rather than the true arrangement of atoms, this discrepancy suggests that density-of-states peaks are somewhat displaced from the location of As dimers in the ⟨110⟩ direction. Calculations by Ohno [46] for a three As dimer model give a similar result. This might explain in part the failure of the three As dimer model in interpreting STM images in earlier work.

Another possible reason was measuring the width of brightly imaged ⟨110⟩-oriented As dimers which was assumed — incorrectly — to be proportional to the number of dimers in the unit cell, whereas in actual fact the STM images were insufficiently resolved to observe individual dimers. That is, this procedure was inherently incorrect. Besides, a correct interpretation of the image requires that the number of crests and troughs in the unit cell be carefully analysed.

We were able to establish a simple STM interpretation rule, applicable even at poor resolutions, by noting how the number of As dimers in the 2 × 4 cell at the outer side of the surface layer depends on the step kink geometry. Since an As-dimer kink results from the transverse translation by $\mathbf{a}_0$ along ⟨110⟩, it follows that if 2 × 4 and c(2 × 8) cells consist of three As dimers (Fig. 6a and 6b), As dimer images should also appear continuous in the kink region, whereas in the two As-dimer case (Fig. 6c and 6d), the unit cell spacing must be $\mathbf{a}_0$. Using this rule and the results of the structural study of the kink, the three As dimer 2 × 4 model was dropped from consideration. We found that the three-dimer scheme does not in fact stand this test for any of the published STM images and should therefore be replaced by the two-dimer model.

Within the β phase (Fig. 5b), the dimer vacancy rows are straight for an average of over 300 A along the $\langle\bar{1}10\rangle$ direction before each kink. The kinks themselves tend to align along ⟨110⟩ and form large domains that extend for up to 3000 A in this direction, showing β to be a well-ordered phase [41]. In the α phase (Fig. 5a), the vacancy rows are interrupted by $\langle\bar{1}10\rangle$-oriented kinks at regular intervals of several dimer lengths. The kinks align along the ⟨110⟩ direction in much the same way as in β. The α domains are typically 60 A and 500 A across in the $\langle\bar{1}10\rangle$ and ⟨110⟩ directions, respectively. In the γ phase, the density of kinks along $\langle\bar{1}10\rangle$ is very much as in the α, except that the kinks are arranged chaotically and exhibit no ⟨110⟩ order characteristic of α. The γ phase also has a considerable number of open regions, which have no As dimers in the top layer and in which the structure of the lower-level terrace is discernible. The γ domain dimensions in Fig. 5c depend on growth details and are about 60 A and 100 A in the $\langle\bar{1}10\rangle$ and ⟨110⟩ directions, respectively.

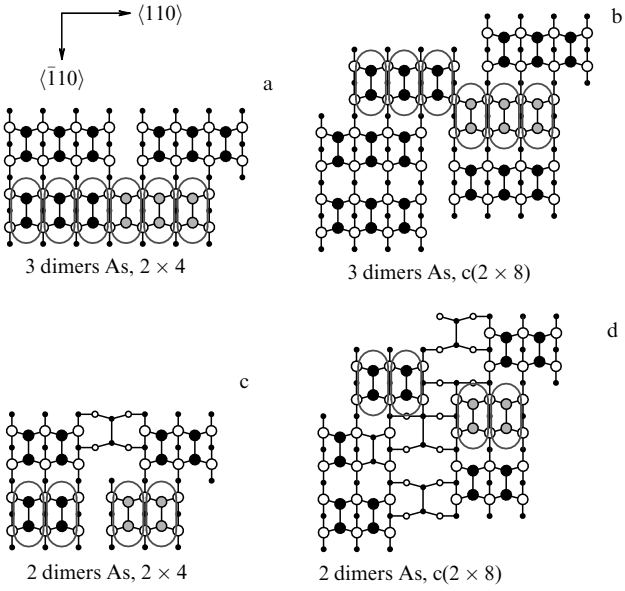


**Figure 6.** STM image atomic arrangements illustrating the relation between the positions of the step kinks and As dimers for the $2 \times 4$ and $c(2 \times 8)$ phases, based on the two and three As dimer models. For the unit cell of three As dimers, the dimers are in contact with adjacent As dimers located near the kinks; for the unit cell of two As dimers, the dimer separation equals the width of the As dimer.

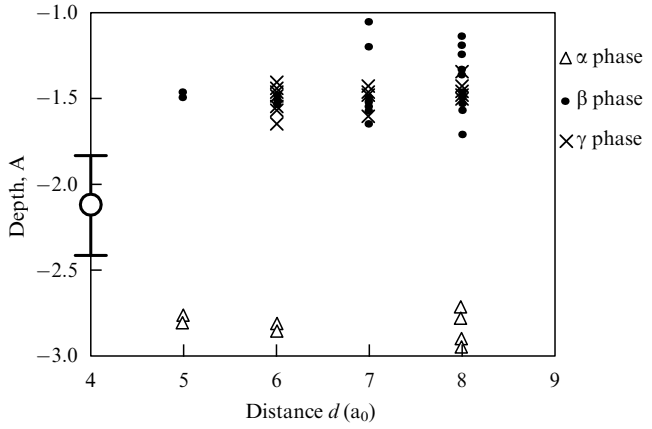


**Figure 7.** Depth of the dimer vacancy region (as measured from the upper layer of As dimers) versus the magnitude of the interval $d$ (in units of $\mathbf{a}_0$) for three various phases.

We also examined the distribution of the quantity $d$, the cell spacing along $\langle 110 \rangle$. For β, the dominant interval was found to be $d = 4\mathbf{a}_0$ (98%), $d = 3\mathbf{a}_0$ and $5\mathbf{a}_0$ contributing $< 1\%$ each. The result for α was almost the same, the somewhat larger fractions of $3\mathbf{a}_0$ (8%) and $5\mathbf{a}_0$ (4%) indicating a somewhat higher kink density compared to β. For γ, the $d$ distribution varied widely with the preparation conditions. The $d$ distribution for the surface in Fig. 5c was found to be as follows: $4\mathbf{a}_0$, 63%; $7\mathbf{a}_0$, 15%; $3\mathbf{a}_0$, 8%; $5\mathbf{a}_0$, 3%; beyond $7\mathbf{a}_0$, 11%. This is clear evidence that the γ phase consists of small $2 \times 4$ regions separated by open regions of typical dimension $d = 7\mathbf{a}_0$.

The quantitative analysis of STM data may also provide useful information on near-surface structures. The STM image depth profiles measured along $\langle 110 \rangle$ for the α, β, and γ phases show considerable differences, especially between α and the other two phases. Whereas the α phase (see the profile in Fig. 5a) usually shows no features between the dimers, in the dimer vacancy phases β and γ (see the profiles in Fig. 5b and 5c) one or two weak step lines are systematically observed. The profile depth results on the As dimer vacancy are summarized in Fig. 7, in which the depth profile measured from the location of As dimers in the top surface layer is plotted as a function of the $2 \times 4$ cell spacing $d$, and which shows that the depth $h$ for a regular $2 \times 4$ region at $d = 4\mathbf{a}_0$ is $2.1 \pm 0.3$ A for each of the phases α, β, and γ. The fact that this is substantially lower than the expected value of the depth of the double GaAs(001) layer $h = 2.8$ A can be attributed to the so-called tip effect: the vacancy depth-to-width ratio in this case is too large for the bottom of a dimer vacancy to be reflected. However, when this interval was sufficiently large, $d > 5\mathbf{a}_0$, a reasonable value of approximately $h = 2.8$ A was obtained for the α, whereas in β and γ the depth was found to be about 1.4 A, half the depth of the double layer $(h/2)$.

In the filled-state regime ($V_s < 0$), which is the one we worked in, As atoms are imaged as steps, whereas Ga dangling bonds are not seen at all. In the $2 \times 4$ models of Fig. 1 none of the structures could produce scanning profiles at As dimer vacancy regions. Thus, the depth $h/2$ seen in the β and γ phases in Fig. 7 implies that in this case an unknown near-surface phase should exist in the vacancy region. Results of such observations provide information necessary for the study of near-surface structures.

### 4.2 Dynamical RHEED analysis of the $2 \times 4$–α, β, γ phases

In order to develop a better understanding of the formation of the α, β, γ phases, and recognizing the insufficiency of kinematic analysis alone, we performed RHEED intensity computations for various $2 \times 4$ models using the dynamic theory of Ichimiya [57]. Although the dynamical (i.e., multiple electron scattering) effects are known to be crucial for the analysis of the GaAs(001) surface [14], to date no systematical dynamical RHEED analyses have been conducted because of the lack of detailed information on the surface structure [43]. Our calculations included 19 zeroth order Laue zone beams in the incidence direction $\langle \bar{1}10 \rangle$. Since the RHEED intensities in the zeroth Laue zone are insensitive to displacements across the beam incidence direction, the relaxation along $\langle \bar{1}10 \rangle$ was neglected [57].

The basic structural models used in the analysis are shown in Fig. 1a–f. We generally assumed that As dimers are contracted by 0.2 A perpendicular to the surface (in order that the As–Ga bond length remain unchanged by dimerisation) and that they have no need for displacement along $\langle 110 \rangle$. Other atoms were assumed not to relax from their bulk equilibrium positions. The influence of small atomic displacements on the RHEED intensity was also examined. Specifically, the rocking curves (i.e., curves of the intensity of elastically diffracted beams as a function of the primary electron beam angle of incidence) were calculated for (0 0), (0 1/4), (0 1/2), (0 3/4), and (0 1) zeroth order Laue zone beams, with the intensities obtained by averaging within the incidence angle $\pm 0.2°$. To illustrate the results, a set of rocking curves for Chadi's two As-dimer model are shown in Fig. 8a–e. The parameters used in the dynamical calculations for this model are summarized in Fig. 8f. The

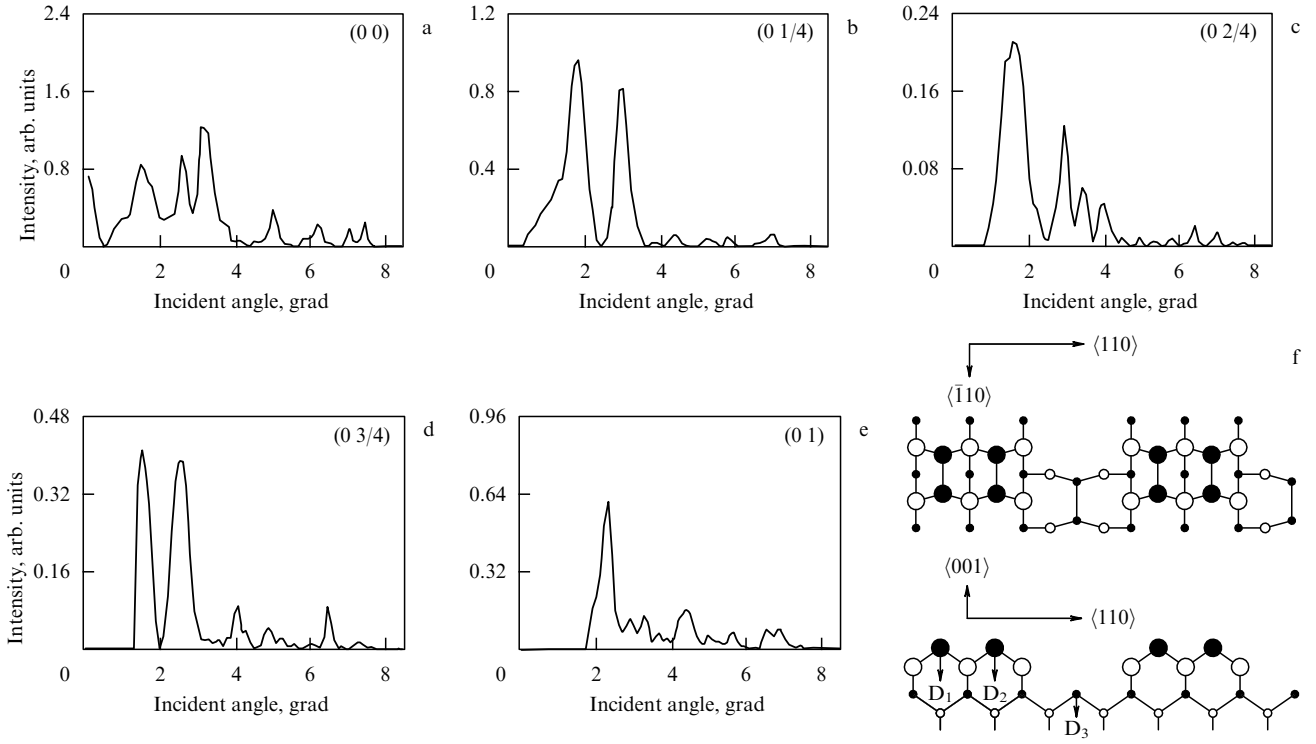


**Figure 8.** Rocking curves for (a) (0 0), (b) (0 1/4), (c) (0 2/4), (d) (0 3/4), and (e) (0 1) reflections as calculated from Chadi's [53] two dimer model. In (e) the parameters of the model of Fig. 1b used in dynamical RHEED calculations are listed. Filled (open) circles denote As (Ga) atoms. The top and side views are shown. The contraction of dimers (two in the upper layer and one in the third layer) is 0.2 A.

rocking curves in Fig. 8 agree well with our measurements at 10 keV and with the data of Larsen et al. [58], some angular shifts being due to the beam energy difference (Larsen's experiments were made at 12.5 keV). The important point is that small variations of these parameters had little or no effect on the relative intensities. Besides, it was clearly demonstrated that the observation of the 2/4 and 3/4 reflections requires incident angles in excess of 0.8° and 1.3°, respectively, which further testifies against FP's small incident angle approach [15].

The RHEED patterns for the α, β, and γ phases were obtained at room temperature (Fig. 9) and correspond to the STM images of Fig. 5. The RHEED data were processed so as to allow comparison with theoretical predictions and are represented by histograms in Fig. 9a–c for the α, β, and γ phases, respectively. The 2/4 order reflection was weak for the α and relatively strong for β (compared to 1/4 and 3/4) but absent in the γ phase; all this being consistent with the results of Ref. [15].

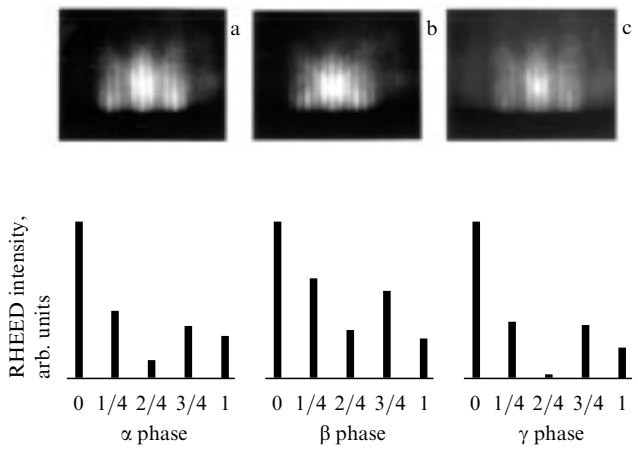


**Figure 9.** Experimental RHEED patterns for the α, β, and γ phases and the measured intensity profile broadening for (a) α, (b) β, and (c) γ phases.

Figure 10 is a summary of our reflection intensity results. Calculations for the two As-dimer model of Fig. 1b were performed for both cases, (i) neglecting surface relaxation (Fig. 10b), and (ii) including the surface relaxation mechanism of Ref. [48] (Fig. 10c). For FP's two As-dimer model of α, the following versions were considered: Chadi's [44] model illustrated in Fig. 1c, without dimerisation or relaxation in the second Ga layer (Fig. 10d); FP's [15] model illustrated in Fig. 1d, with dimerised but not relaxing second Ga layer (Fig. 10e); and NF's [47] model of Fig. 1e with full relaxation (Fig. 10f). In Figure 10h, the results for this model including the second layer effect are also shown.

Chadi's three As-dimer model (Fig. 1a) yields a weak 3/4 reflection (Fig. 10a) compared to kinematic calculations [15]. Varying the As dimer contraction from −0.4 to −0.5 A showed no noticeable intensity change. The inward relaxation of second layer Ga atoms with dangling bonds (to 0.8 A) also contributes little to 1/4 and 2/4 intensities and does not agree with experimental results. More importantly, however, the three-dimer unit cell is inconsistent with the STM images of the α, β, and γ phases shown in Fig. 5.

McCoy et al. [19] analysed the $2 \times 4$ unit cell using the dynamical RHEED theory to fit the measured rocking curves. The best fit was given by Chadi's three-dimer model (Fig. 1a) corrected for the relaxation of the first- and second-layer atoms. It was found that the central As dimer contracts by 0.2 A in the direction normal to the surface (with the

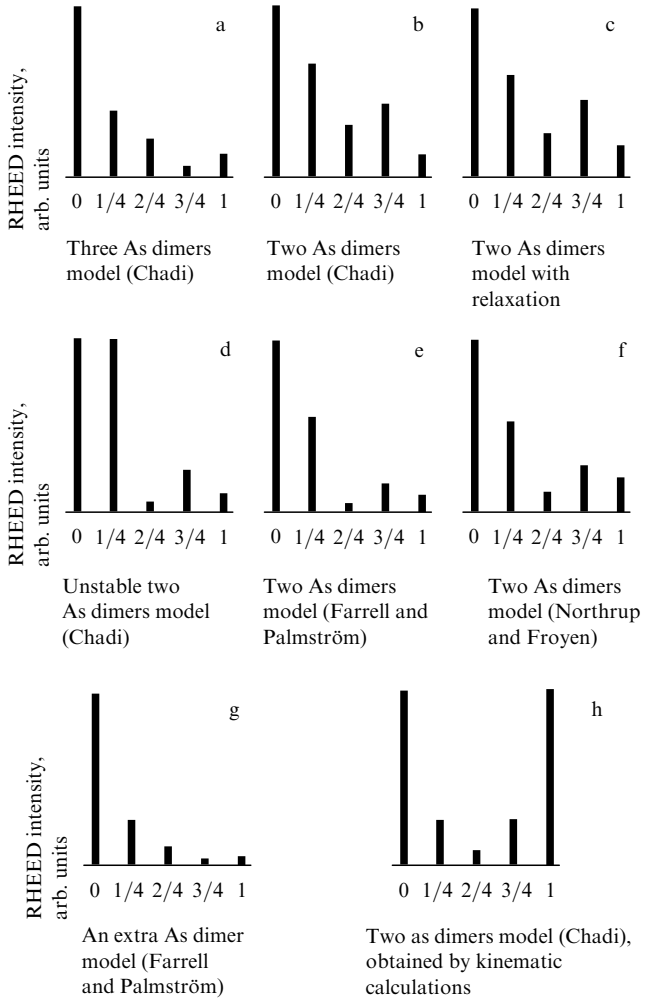


**Figure 10.** RHEED intensity profiles calculated for various surface structure models (Fig. 1) using dynamic theory (a – g) and the kinematic approximation (h).

surface being 'buckled' as a result) and that the second-layer Ga atoms may relax both in and normal to the plane [19]. In McCoy's opinion, the surface buckling is consistent with the STM data of Gallagher et al. [40]. Note, however, — a fact Gallagher and coworkers do not mention explicitly — that the step spacing in their high-resolution STM images is readily measured and is found to be about 5 A. On the other hand, the terraces due to McCoy's buckling [19] are separated by $2\mathbf{a}_0 = 8.0$ A, inconsistent with the STM results. In his dynamical-analysis fitting of fractional-order reflections, McCoy employed normalised curves and neglected the absolute value of the reflection intensity. Although both the normalised intensities and the positions of peak features in his fitted curves agree well with the experimental rocking curves, the reflection intensities obtained from the fitted atomic positions were close to those for Chadi's three-dimer no-relaxation cell. Most importantly, though, changing atomic coordinates yielded only one fourth of the $2 \times 4$ reflection intensity given by Chadi's model (Fig. 10a). Note that this is but just one example of the confused state of affairs we discussed in the Introduction and are now trying to resolve! The additional dimer model shown in Fig. 1g [15] predicts only a weak 3/4 reflection — as was the case with the three-dimer model of Fig. 1a — and does not agree with the experimental data at all.

The two-dimer As model of Chadi (Fig. 1b) gives nearly identical intensities for the fractional order 1/4, 2/4, and 3/4 features (Fig. 10b) and agrees well with the β phase (Fig. 9b). Varying the As dimer contraction from −0.4 to −0.5 A yields a change of about 20% in the intensity of the zeroth reflection, the best fit being achieved at about −0.2 A. The kinematic calculations for this model with only the first layer taken into account recovered the results from the two As dimer model of FP [15] and in particular yielded zero intensity for the 2/4 order reflection. Since the second layer contains only three of the four Ga pairs, however, it follows that the beams diffracted on the first plane will diffract again on the second and that the first- and second-layer reflections will interfere thus making the intensity of the reciprocal lattice vectors to oscillate in a sinusoidal manner as a function of the reciprocal lattice coordinate normal to the surface $(k_z)$ [59]. For a less ordered surface, the image intensities of the reciprocal lattice vectors must be averaged, giving values similar to those shown in Fig. 10h. The averaged (0 0), (0 1/4), (0 1/2), (0 3/4), and (0 1) reflection intensities obtained from kinematic calculations using Chadi's two As dimer model have values of 13, 3, 1, 3, and 13, respectively (Fig. 10h) and can be treated as the sum of values obtained in the kinematic approximation for the two-dimer (4, 2, 0, 2, 4) and three-dimer (9, 1, 1, 1, 9) unit cells. As a result, even in the kinematic approximation we obtain a nonzero 2/4 reflection intensity for Chadi's two-dimer cell. The dynamical effect increases the 2/4 reflection intensity still further, bringing it into agreement with the data on the β phase (Fig. 9b).

Recently, NF [48] have extended their *ab initio* calculations to Chadi's two As-dimer model. Taking advantage of the surface atom coordinates revised by Northrup, we also carried out reflection intensity calculations (see Fig. 10c). We found that our results deviate little from the original model (Fig. 10b) and that our method is not sensitive to exact atomic positions, indicating that it is the general arrangement of atoms in each atomic layer which determines the situation as a whole. Our computed rocking curves showed a good agreement with the experimental curves of McCoy [19] in both peak positions and absolute reflection intensities.

Two As dimer models with four second layer Ga pairs that were developed by Chadi (Fig. 10d) [44], FP (Fig. 10e) [15], and NF (Fig. 10f) predict a weak 2/4 feature, in general agreement with the 2/4 reflection intensity of the α phase (Fig. 9a). At the same time the intensity of the 1/4 reflection was found to be very sensitive to the dimerisation of the second layer Ga atoms (Fig. 10d and 10e) and changed from 1.0 to 0.25 relative to the zeroth reflection as the Ga spacing was varied from 4.0 A (Fig. 10d) [44] to 3.9 A. Because reflection intensities are not very sensitive to the relaxation of second-layer Ga atoms (barring their dimerisation), it would be incorrect if the difference between FP's (Fig. 10e) [15] and NF's (Fig. 10f) [47] unit cells were discussed based on reflection intensity data alone: a detailed analysis of the rocking curves is also necessary [19, 54, 60]. Such an analysis gave support to the NF model which, as far as the α and β phases are concerned, agrees well with the profile depth data of Fig. 7.

As for the γ phase, with its domain spacing of typically $d = 7\mathbf{a}_0$, kinematic calculations are justified by the weak dynamic effects, and the RHEED pattern must and does

show a less intensive 2/4 feature (Fig. 10h), not inconsistent with experimental data (Fig. 9c).

### 4.3 Surface phase transitions between the c(4 × 4) and 2 × 4−γ lattices

In order to investigate the structure of open regions in the 2 × 4−γ phase, c(4 × 4) and 2 × 4−γ phases and mixtures of them were prepared by MEE. The STM image in Fig. 4a is representative of the MEE-grown c(4 × 4) phase. The unit cell of the structure has periods $4\mathbf{a}_0$ and $2\mathbf{a}_0$ along $\langle\bar{1}10\rangle$ and $\langle 110\rangle$, respectively, and possesses a c(4 × 4) symmetry. The most commonly used c(4 × 4) model due to Biegelsen [36] (Fig. 11a) consists of three As dimers which involve the As atoms of the c(4 × 4) cell and form a double As layer. To compare our STM results with this model the profile depth of the c(4 × 4) was plotted as a function of distance along the $\langle\bar{1}10\rangle$ (Fig. 11b) and $\langle 110\rangle$ (Fig. 11c) directions. Below (Fig. 11d), a similar plot for the profile depth of (2 × 4)−γ(β) is given for comparison, which clearly shows two (not three!) peaks $2\mathbf{a}_0$ apart along the $\langle\bar{1}10\rangle$ direction. This is consistent with Biegelsen's model [36] which assumes the electronic density of states to be higher near the corner As dimers. The step periodicity along the $\langle 110\rangle$ scanning profile depth (Fig. 11c and 11d) is also consistent with this model. Thus, STM analysis generally supports the Biegelsen model, even though c(4 × 4) is admittedly not perfectly ordered [43] and the number of As dimers per cell may be two or even three (analogous to the absence of dimer defects in the 2 × 4 phases). We also observed As dimer displacements by $\mathbf{a}_0$ along the $\langle 110\rangle$ direction (similar to the repeated step kinks in 2 × 4), and local $p(2 \times 2)$ regions with the two As-dimer cell, which were first reported by Biegelsen [36]. By varying the number of As dimers, the X-ray diffraction experiments [29] can also be readily explained.

Comparing the width of the dimer images along the dimerisation direction in the c(4 × 4) (Fig. 11c) and 2 × 4 (Fig. 1d) phases, it is apparent that the As dimers in the former are narrower than those in the latter. Hence the marked difference in the STM images of the As dimers in 4 × 4 and 2 × 4, which are seen as small round steps and usual elongated steps in these respective phases. This difference between the spatial distributions of the dangling-bond electronic states is, in our view, due to the different chemical environment of As dimers in the c(4 × 4) and 2 × 4 phases which leads, ultimately, to very different STM images. Note also that the As dimers in c(4 × 4) are associated with As atoms, so that the charge transfer from the second to the first layer is not considered, and the surface As dimers remain neutral. In contrast, the As dimers in 2 × 4 involve Ga atoms, and in this case the charge transfer from the second layer is invoked and consequently the charging of As dimers takes place. The difference in the electronic density of states was investigated in photoelectron spectroscopy studies by Larsen and co-workers [26]. A peak feature they observed in 2 × 4 surface states was larger in amplitude but lower in energy than that for c(4 × 4), which is consistent with the size difference between the STM images of As dimers in the γ, β, and c(4 × 4) phases.

The explanation of the difference between the STM images of As dimers in a c(4 × 4) or a 2 × 4 cell made possible an understanding of the mechanism of the structural transition from c(4 × 4) to 2 × 4−γ on less As-rich surfaces. Note here that even the c(4 × 4) phase displayed incipient islands with the 2 × 4 unit cell (Fig. 4a). For island growth with somewhat less As, more regions of 2 × 4 were seen (Fig. 4b–d). A number of MEE experiments at various $[As_4]$/[Ga] ratio values confirmed that 2 × 4 regions become dominant and are ultimately identified with the γ phase grown with normal MBE at an $[As_4]$/[Ga] ratio of 12:1 (Fig. 5c). As seen in Fig. 4, there are still c(4 × 4) regions remaining between incipient 2 × 4 islands. These observations naturally led to the conclusion that the 2 × 4−γ phase results from replacing c(4 × 4) by 2 × 4 cells of lower As content. Indeed, close examination of the open areas in the γ (Figs 5c, 7, and 12a) showed a large number of subsurface structures at a depth of about 1.4 A (i. e., $h/2$, half the width of the second layer). One further point which is clear from Fig. 5c is that the most ordered phase is γ and that the presence of chaotically distributed open areas results in the formation of small domains about 60 A and 100 A across. A detailed investigation of some of the open areas of γ for the intervals $d = 5\mathbf{a}_0$, $7\mathbf{a}_0$, and $8\mathbf{a}_0$ revealed that these areas contain the remaining As dimers that are located in the third layer of As atoms similar to the double As layer in c(4 × 4). In the open areas in Fig. 12a one also can see dim lines (marked with arrows) running along the $\langle\bar{1}10\rangle$ direction 1.4 A ($h/2$) below the top As dimer layer (e.g., line A). The profile analysis of the STM images of the α, β, and γ phases (Figs 5 and 11) showed that at the surface under study the grooves with $d \geqslant 5\mathbf{a}_0$ have the same depth $h$ seen for the α phase, and a depth $h/2$ for β and γ, allowing the existence of structural differences between the second and/or third layer. Based on the analysis of the STM data (Figs 5c and 12a), we were able to construct structural models for the open area of the γ with an interval $d = 7\mathbf{a}_0$ (Figs 12b, c). The relative importance of individual structures depends on the preparation conditions: for example, the structure of Fig. 12b is found to prevail in more than 90% cases for $d = 7\mathbf{a}_0$, whereas narrow open areas with $d = 5\mathbf{a}_0$ constitute as little as a few percent.

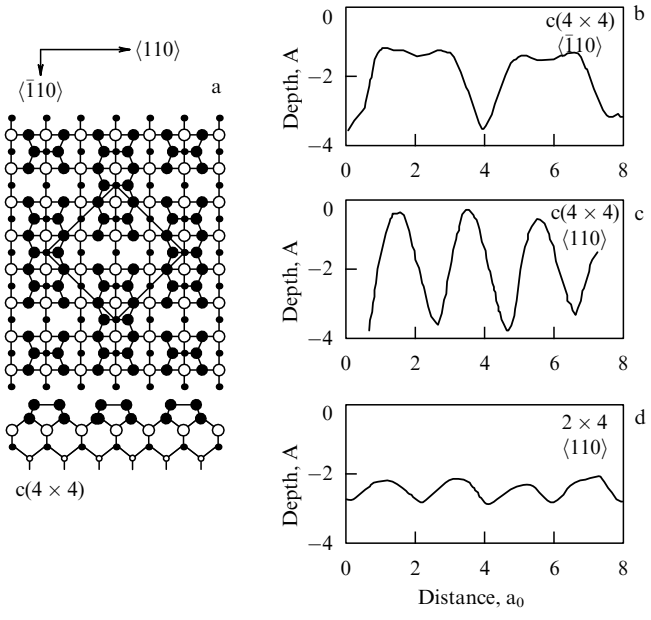


**Figure 11.** (a) Biegelsen's [36] model of the c(4 × 4) phase, top and side views. Filled (open) circles denote As (Ga) atoms. Also shown are profile depth plots for c(4 × 4) along $\langle\bar{1}10\rangle$ (b) and $\langle 110\rangle$ (c), and for 2 × 4 along $\langle 110\rangle$ (d).

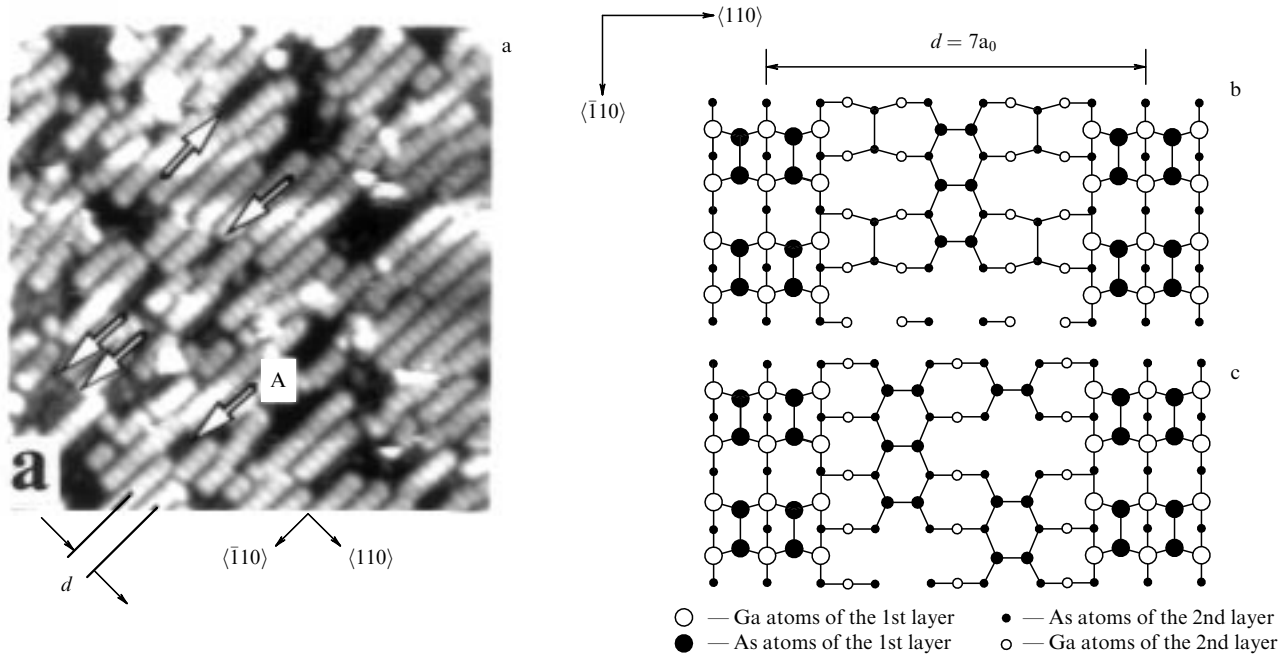


**Figure 12.** (a) STM image of a 260 A × 260 A area of the γ phase, $V_s = -3.0$ V, $I_t = 2.0 \times 10^{-11}$ A. (b) and (c) show structural models of an open area of γ with the interval $d = 7\mathbf{a}_0$.

## 5. Structural models for the two-dimensional $2 \times 4-\alpha$, β, and γ phases

Based on our STM results and the dynamical RHEED intensity calculations, we propose the following unified model of the structure of the $2 \times 4-\alpha$, β, and γ phases (Fig. 13): the α phase is described by the two-dimer As model of FP [15] modified by the inclusion of NF's [47] surface relaxation; for the β, the two As- dimer model of Chadi [44] is adequate; and the γ phase may be simply treated as a mixture of β and $c(4 \times 4)$.

Because of the considerable As transfer both to and along the surface during MBE, the surface growth was quasi-stationary, and removing As atoms was in fact equivalent to adding Ga atoms. For γ, an open area with a local double layer of As has an As surface coverage of no more than 1.75 ML, the same as $c(4 \times 4)$, whereas for a $2 \times 4$ area we have 0.75 ML (i.e., one As dimer per unit cell in the third layer). Thus, the amount of As coverage in γ and in the $c(4 \times 4)/2 \times 4-\gamma$ mixture ranges between 0.75 and 1.45 ML, but both the surface stoichiometry and the $c(4 \times 4)$ to $2 \times 4-\gamma$ domain ratio are unambiguously determined by specifying the sample preparation conditions. The As coverages in the $2 \times 4-\alpha$; β; γ, and $c(4 \times 4)$ phases are 0.5, 0.75, 1.0, and 1.75 ML, respectively, in excellent agreement with previous results.

Finally, we note that the structural model we propose here for the $c(4 \times 4)$ and $2 \times 4-\alpha$, β, and γ phases is also adequate in explaining the recent medium-energy ion scattering data of Falta et al. [34] if one assumes that Ga atoms exposed to an ion beam increase their surface ordering from $c(4 \times 4)$ successively to the γ, β, and α phases. However, the ions that are backscattered by substrate atoms when escaping the crystal may be shadowed by surface atoms (the so-called blocking effect). The discrepancy between Falta's results and the top As layer models, discussed in Section 2, relates to the absolute value of the As/Ga intensity ratio for the $2 \times 4-\alpha$ phase [34]. However, in the two As dimer model of the α phase all As dimers of the first layer as well the Ga atoms of the second and As atoms of the third turn out to be displaced from their original positions; this is expected to reduce the blocking effect of the sixth layer Ga atoms on the scattering intensity, especially outside the shadow cone.

## 6. Conclusions

The physics of multicomponent surface phases is currently developing at a very fast rate owing to advances in epitaxial growth technology for micro- and nanoelectronic structures [4]. There has been a marked increase in the number of theoretical works on models of MBE-grown structures [15–19, 46–48] (for which the most effective diagnostic tool is undoubtedly STM).

Our original MBE-STM apparatus has allowed a detailed investigation of atomic structures arising on the MBE-grown GaAs(001)$-2 \times 4$ surface, which showed that the phases $2 \times 4-\alpha$, β, and γ in the outer surface layer all have the same unit cell consisting of two As dimers and two As-dimer vacancies. Based on STM and RHEED data and dynamical RHEED intensity calculations, a unified scheme is proposed in which the α phase is described by the two-dimer As model of Farrell and Palmström [15] including surface relaxation [47] and with a coverage of 0.5 ML; the β phase is described by the two As-dimer model of Chadi [44], with an As coverage of 0.75 ML; and the γ is a mix of β and $c(4 \times 4)$, with an As coverage varying between 1.75 and 0.75 ML depending on the growth conditions.

On the other hand, the extensive information that has been gathered on MBE-grown atomic structures in recent years is only now starting to be reliably interpreted. Since, as the present review has demonstrated, even such a powerful technique as STM does not necessarily ensure an unequivocal

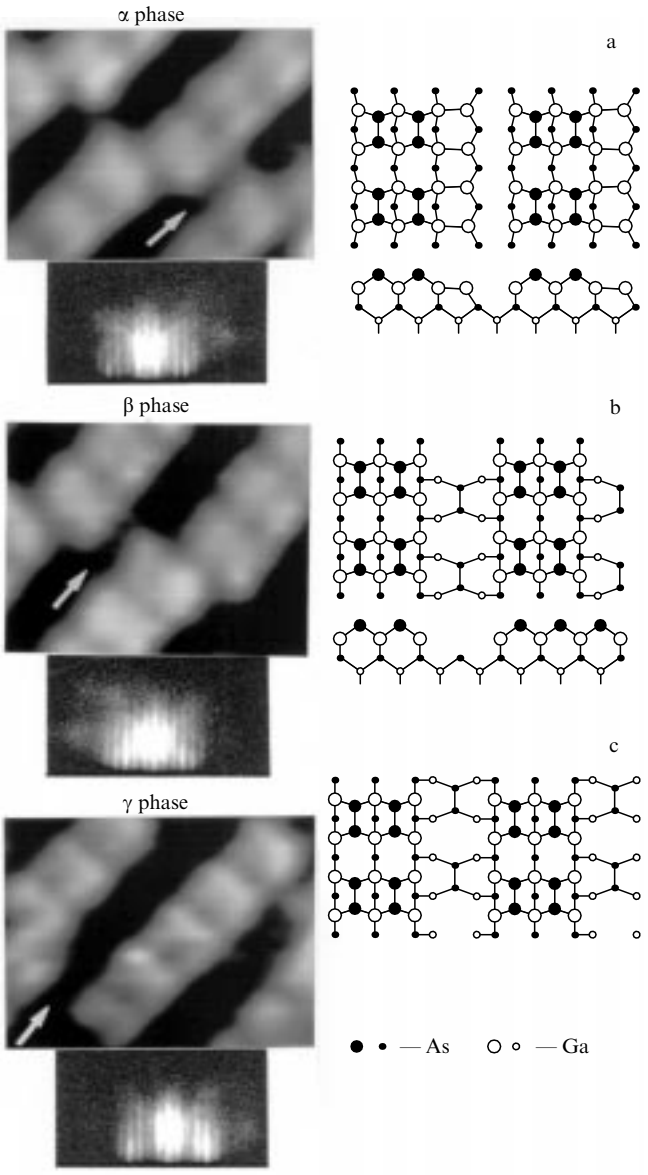


**Figure 13.** STM images and RHEED patterns of the GaAs(001) surface with structural models for the α (a), β (b), and γ (c) phases.

interpretation of the experimental data, the most promising approach is to combine the *in situ* STM technique with other methods available for the study of the surface structure of solids, such a RHEED [15 – 18], LEED [21], various electron spectroscopy techniques [25 – 28, 31 – 33], medium-energy ion scattering [34], etc., which, of course, should always go in parallel with a search for new theoretical models capable of describing the complex phenomena accompanying epitaxial growth and the formation of atomic surface structures of various types.

**Acknowledgements.** We would like to thank Professor A Ichimiya for assistance in carrying out dynamical RHEED computations, Dr. J E Northrup for helpful discussions and communicating to us his theoretical results, and Prof. J -M Zhou for his useful comments and assistance. R Z Bakhtizin was supported in part by the Russian Federation Program "Surface Atomic Structures" under Project No 96-2.27 and by ISSEP under Grant No 926p.

## References

1. Madhukar A, Ghaisas S V *CRC Crit. Rev. Solid State Mater. Sci.* **14** 1 (1988)
2. Herman M A, Sitter H *Molecular Beam Epitaxy: Fundamental and Current Status* (New York, Berlin, Heidelberg: Springer-Verlag, 1996)
3. Cho A Y (Ed.) *Molecular Beam Epitaxy* (New York: AIP Press, 1994)
4. Bakhtizin R Z et al. *Zh. Eksp. Teor. Fiz.* **111** (5) 1858 (1997); [*Sov. Phys. JETP* **84** 1016 (1997)]
5. Sakaki H, Node H (Eds) *Nanostructures and Quantum Effects* (Berlin, Heidelberg: Springer-Verlag, 1994)
6. Cho A Y *J. Appl. Phys.* **42** 2074 (1971); Arthur J R *Surf. Sci.* **43** 449 (1974)
7. Cho A Y, Arthur J R *Prog. Solid State Chem.* **10** 157 (1975)
8. Cho A Y *J. Appl. Phys.* **47** 2841 (1976)
9. Neave J H, Joyce B A *J. Cryst. Growth* **44** 387 (1978)
10. Larsen P K et al. *Phys. Rev. B* **27** 4966 (1983)
11. Joyce B A et al. *Phys. Rev. B* **29** 814 (1984)
12. Farrell H H, Harbison J P, Peterson L D *J. Vac. Sci. Technol. B* **5** 1482 (1987)
13. Knibb M G, Maksym P A *Surf. Sci.* **195** 475 (1988)
14. Larsen P K, Chadi D J *Phys. Rev. B* **37** 8282 (1988)
15. Farrell H H, Palmström C J *J. Vac. Sci. Technol. B* **8** 903 (1990)
16. Däweritz L, Hey R *Surf. Sci.* **236** 15 (1990)
17. Yamaguchi H, Horikoshi Y *Phys. Rev. B* **44** 5897 (1991)
18. Deparis C, Massies J *J. Cryst. Growth* **108** 157 (1991)
19. McCoy J M et al. *Phys. Rev. B* **48** 4721 (1993); *Surf. Sci.* **261** 29 (1992)
20. Nörenberg H, Koguchi N *Surf. Sci.* **296** 199 (1993)
21. Van Bommel A J, Crombeen J E, van Oirschot T G *Surf. Sci.* **72** 95 (1978)
22. Drathen P, Ranke W, Jacobi K *Surf. Sci.* **77** L162 (1978); Ranke W, Jacobi K *Prog. Surf. Sci.* **10** 1 (1981)
23. Svensson S P, Nilsson P O, Andersson T G *Phys. Rev. B* **31** 5272 (1985)
24. Massies J et al. *Surf. Sci.* **99** 121 (1980)
25. Duszak R et al. *J. Vac. Sci. Technol. B* **10** 1891 (1992)
26. Larsen P K, Neave J H, Joyce B A *J. Phys. C* **14** 167 (1981)
27. Larsen P K et al. *Phys. Rev. B* **26** 3222 (1982)
28. Chiang T C et al. *Phys. Rev. B* **27** 4770 (1983)
29. Sauvage-Simkin M et al. *Phys. Rev. Lett.* **62** 563 (1989)
30. Chambers S A *Surf. Sci.* **261** 48 (1992)
31. Kamiya I et al. *Phys. Rev. Lett.* **68** 627 (1992); *Phys. Rev. B* **46** 15894 (1992)
32. Frankel D J et al. *J. Vac. Sci. Technol. B* **5** 1113 (1987)
33. Kanisawa K et al. *J. Cryst. Growth* **115** 348 (1991)
34. Falta J et al. *Phys. Rev. Lett.* **69** 3068 (1992); "Comments and reply" *Phys. Rev. Lett.* **70** 3171 (1993)
35. Pashley M D et al. *Phys. Rev. Lett.* **60** 2176 (1988)
36. Biegelsen D K et al. *Phys. Rev. B* **41** 5701 (1990); *Proc. SPIE* **1186** 136 (1990)
37. Pashley M D, Haberern K W *Phys. Rev. Lett.* **67** 2697 (1991); Pashley M D et al. *Phys. Rev. B* **48** 4612 (1993)
38. Heller E J, Zhang Z Y, Lagally M G *Phys. Rev. Lett.* **71** 743 (1993); Heller E J, Lagally M G *Appl. Phys. Lett.* **60** 2675 (1992)
39. Wassermeier M et al. *Surf. Sci. Lett.* **278** L147 (1992); Bressler-Hill V et al. *J. Vac. Sci. Technol. B* **10** 1881 (1992)
40. Gallagher M C, Prince R H, Willis R F *Surf. Sci.* **275** 31 (1992)
41. Zhou J M et al. *Appl. Phys. Lett.* **64** 583 (1994)
42. Xue Q-K et al. *J. Appl. Phys.* **75** 5201 (1994)
43. Hashizume T et al. *Phys. Rev. Lett.* **73** 2208 (1994)
44. Chadi D J *J. Vac. Sci. Technol. A* **5** 834 (1987)
45. Qian G-X, Martin R M, Chadi D J *Phys. Rev. B* **38** 7649 (1988)
46. Ohno T *Phys. Rev. Lett.* **70** 631 (1993)
47. Northrup J E, Froyen S *Phys. Rev. Lett.* **71** 2276 (1993)
48. Northrup J E, Froyen S *Phys. Rev. B* **50** 2015 (1994)
49. Harrison W A *J. Vac. Sci. Technol.* **16** 1492 (1979)
50. Pashley M D *Phys. Rev. B* **40** 10481 (1989)
51. Horikoshi Y, Kawashima M, Yamaguchi H *Jpn. J. Appl. Phys.* **25** L868 (1986)
52. Sakurai T et al. *Prog. Surf. Sci.* **33** 3 (1990)

53. Miwa Sh et al. *Jpn. J. Appl. Phys.* **32** 1508 (1993)
54. Bakhtizin R Z et al. *Zh. Eksp. Teor. Fiz.* **108** 977 (1995) [*Sov. Phys. JETP* **81** 534 (1995)]; *Zh. Tekh. Fiz.* **64** 113 (1994)
55. Ichimiya A, Kambe K, Lehmpfuhl G *J. Phys. Soc. Jpn.* **49** 684 (1980); Horio Y, Ichimiya A *Surf. Sci.* **219** 128 (1989)
56. Feenstra R M, Stroscio J A, Tersoff J, Fein A P *Phys. Rev. Lett.* **58** 1192 (1987)
57. Ichimiya A *Jpn. J. Appl. Phys.* **22** 176 (1983); **24** 1365 (1985); *Surf. Sci.* **235** 75 (1990)
58. Larsen P K et al. *Surf. Sci.* **169** 176 (1986)
59. Lagally M G, in *Methods of Experimental Physics* (New York: Academic Press, 1985) p. 237; Henzler M *Appl. Surf. Sci.* **11/12** 450 (1982)
60. Karpov I et al. *J. Vac. Sci. Technol. B* **13** (5) 2041 (1995)